Analysis of Traffic Flow in Structured Urban Airspace Networks with MFD-based Feedback Control

Kenny Chour*, Pouria Razzaghi†
Metis Technology Solutions Inc, Moffett Field, CA, 94035, USA.

Dhriti Verma‡
Cornell University, Ithaca, NY 14850, USA.

Min Xue§, Alexey A. Munishkin¶ and Krishna M. Kalyanam‖
NASA Ames Research Center, Moffett Field, CA, 94035, USA

This research delves into applying the Macroscopic Fundamental Diagram (MFD) concept to structured airspace networks for comprehensive aggregate modeling and introduces a feedback-based departure function aimed at optimizing traffic flow. Previous studies have rarely examined structured airspace networks featuring non-stationary vehicles through the MFD perspective. We devised a scenario grounded in practical applications, featuring a multi-lane network with explicit lane-changing behavior. The MFD effectively captured the open-loop response, displaying a low-scatter, unimodal curve on the flow versus occupancy plot. Drawing inspiration from the ground transportation ramp-metering strategies, a proportional-integral-based controller was developed. Extensive simulation outcomes suggest that feedback control, informed by MFD, holds significant potential for managing traffic flow in Urban Air Mobility (UAM) environments; a reduction of 80% in the peak number of vehicles in a holding pattern was observed for a slight reduction in throughput in this study.

I. Introduction

The skyline of our cities is poised for a transformation under the FAA's Urban Air Mobility (UAM) concept by leveraging new types of vehicle for passenger transport and delivery of goods [1]. Under UAM, sustainable vehicle such as Electric Vertical Take-off and Landing (eVTOLs) variants and Unmanned Aerial Systems (UAS) are to be integrated into the U.S. National Airspace System (NAS). These efforts hope to introduce a number of benefits over conventional vehicle such as reduced noise pollution and emissions, circumventing road congestion for users, and increased throughput of trips [2, 3]. However, there is presently little consensus on how to best use the airspace. In a network with structure, such as sky corridors, all vehicle are enforced to stay within the boundaries during flight. This may result in less conflicts and ultimately lead to greater safety in the long term, compared with the free-flight concept. With this focus in mind, the present study aims to develop a macroscopic, aggregate model of a given airspace network, owing to a recent growing trend: applying Macroscopic Fundamental Diagram theory to airspace. Additionally, the present study aims to develop a controller to manage traffic flow and analyze its impact.

The Macroscopic Fundamental Diagram (MFD) is a powerful tool for modeling and analyzing traffic flow on a network level by aggregating known traffic states into a succinct diagram. It was first proposed by Godfrey in 1969 [4] and was empirically proven by Geroliminis and Daganzo in 2008 [5]. Essentially, it illustrates how the accumulation of vehicles influence the overall network capacity and speed, demonstrating that beyond a critical threshold, an increase in vehicular density leads to disproportionate congestion and reduced mobility [6]. The earliest known work applying *fundamental diagrams* to unconventional air traffic was conducted by Jang et al. [7]. The authors investigated different multi-layered lane systems resembling ground transportation networks in the air. After describing a microscopic model (i.e. vehicle dynamics, vehicle control, conflict detection, and conflict resolution behavior), numerical simulations were

*Senior Software Engineer, Metis Technology Solutions, Inc., NASA Ames Research Center, AIAA Member.
†Principal Systems Engineer, Metis Technology Solutions, Inc., NASA Ames Research Center, AIAA Member.
‡NASA OSTEM Intern, Operations Research and Engineering, Cornell University.
§Senior Aerospace Research Engineer, Aviation Systems Division, NASA Ames Research Center, AIAA Senior member.
¶Aerospace Research Engineer, Aviation Systems Division, NASA Ames Research Center, AIAA Member.
‖Senior Aerospace Research Engineer, Aviation Systems Division, NASA Ames Research Center, AIAA Associate Fellow.

conducted with the proposed structures, and the fundamental diagram is used to compare throughput versus density across various structures. Since then, other works have begun to apply the MFD to airspace networks [6, 8–10]. Notably, many of these works either assume the vehicle is always able to hover or move under free-flight airspace.

Going further back, there is an existing body of work that takes inspiration from road traffic flow research and applying it to air traffic. They include concepts such as *kinematic wave theory*, which treats traffic flow as a continuum fluid, while only more recent work has delved into the MFD. Among the earliest known works on treating air traffic as a fluid flow within a continuum was given by Menon et al., which utilized an Eulerian (stationary observer) modeling approach [11, 12] for an interconnected network of one-dimensional control volumes. The authors spatially aggregate air traffic by using the LWR model (Lighthill, Whitham, and Richards), given as a partial differential equation [13]. Through careful simplifications, the model can be recast as a linear, discrete-time system, where linear control theory becomes appropriate. This work is further extended by [14], where a stochastic dynamic model is derived by considering the flow of vehicle between regions and into the airspace. Furthermore, a linear, time-varying stochastic model is provided in [15]. Conventional air traffic however assumes an existing airspace network that is not present with UAS vehicles.

Optimization-based approaches are also another popular paradigm. In [16, 17], UAM traffic is modeled as flows on a directed graph. A nonlinear optimization problem is formulated, which aims to minimize air traffic complexity by optimizing flow along the graph's edges. Due to computational intractability, a heuristic is given by parallel simulated annealing. In [18], a multi-commodity flow formulation was developed to describe flow of vehicle through a vertiport network. The authors varied vertiport topology to study its effect on vehicle throughput. Similarly, a multi-commodity flow formulation is solved in [19] for an airport shuttle air taxi service. Other works utilize a network flow model to schedule flights [20, 21]. A drawback of the aforementioned approaches is computational intractability, which limits the scalability of the methods.

As mentioned, the contribution of this work is two-fold: (i) to create an aggregate model of an airspace network using the MFD methodology, and (ii) to analyze the impact of an MFD-based feedback control on UAM traffic management. Section II discusses the Problem Setting and Formulation, Section III discusses the methodology, while Section IV presents the results and discussion. Concluding remarks are in Section V.

II. Problem Setting and Formulation

The elements constituting a UAM network may be composed of the following primitives: airspace, vertiports, source and sink nodes. Major assumptions for the problem presented in this work are also given as follows:

- All vehicle are to be separated at all times. This is achieved with tactical separation onboard each vehicle.
- Additionally, all vehicle in the corridors are to yield to incoming merge traffic from vertiports via slowing down as much as possible (beyond stall speed) or changing lanes if available.
- Conflict resolution maneuvers are mainly limited to just speed adjustments. However, corridors are considered "porous", i.e. vehicle have the ability to leave the corridor at any time to help resolve conflicts. The same vehicle may also re-enter the corridor, if it can do so safely.
- A rudimentary form of strategic de-confliction is used. Traffic from vertiports may only depart if they respect separation with respect to earlier departures and vehicles upstream in a corridor. Vehicles will remain at vertiports until they can actually depart without violating separation minima, i.e. ground delay pattern is used.
- Level flight is considered in this work.

There are various ways in which airspace corridors may be structured: (i) A sky corridor may contain a single center-line for which all vehicle must travel along, (ii) or it may be composed of several adjacent lanes, for which all vehicle may use to travel along in a specified direction, or (iii) the corridor may have no notion of lanes, instead vehicle may fly through the corridor without a prescribed lane as long as separation is maintained. In the present work, only the single and multi-lane variants are considered.

A source node will introduce vehicle into the UAM network at a prescribed in-flow rate towards some target sink node. The source node's out flow is subject to some known demand model, which is motivated by traffic demand as seen on road freeways. Sink nodes on the other hand will remove vehicles from the network as they complete their trips.

A vertiport can act as both a source or sink node, i.e. vehicle may be introduced into (*spawn*) or removed (*despawn*) from the UAM network. Unlike generic source nodes, vertiports can control the in-flow rate of vehicle departures, as well as out-flow rate of vehicle arrivals. Typically, vertiports may be subject to capacity limits, and as such, cannot handle unlimited arrival rates. Several demand-capacity balancing (DCB) algorithms have been proposed [22, 23], which discretize the operational time horizon into time-bins of specified capacity. vehicle are only allowed to depart if the desired time-bin capacities are not exceeded; else, vehicle are subjected to a ground-delay. In general for airborne vehicle, they may be subject to an airborne hold to limit arrival rates to a vertiport. In the present study, vertiports do not have a capacity limit.

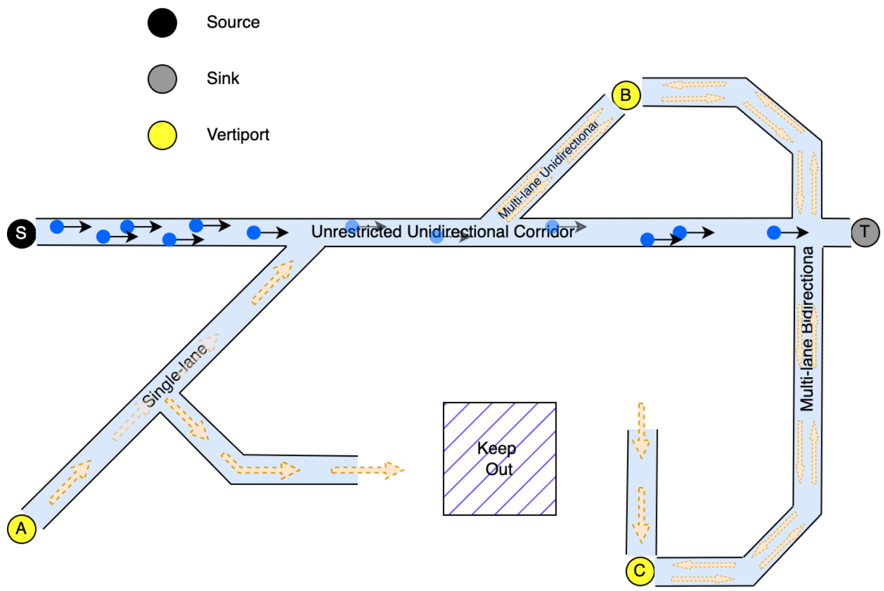

(a) Example of a UAM network with various corridor types and unstructured airspace.

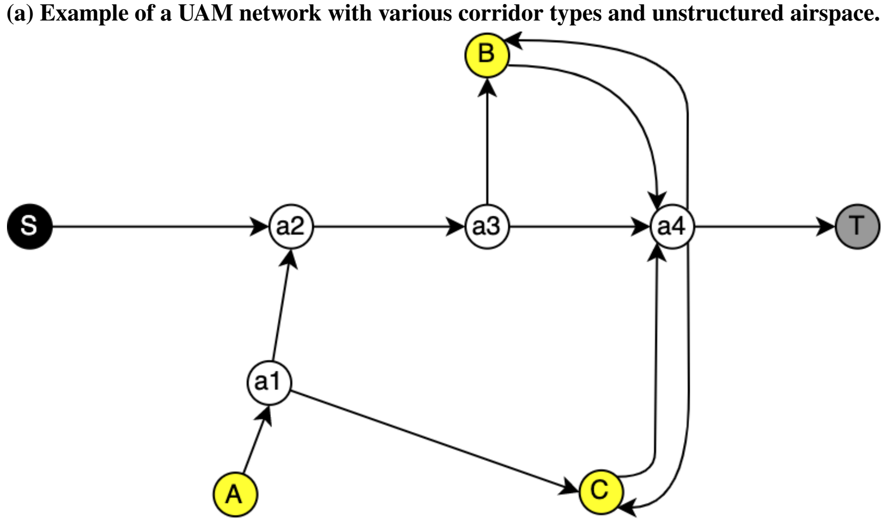

(b) Graph model for a given UAM network with various corridor types and unstructured airspace.

Fig. 1 Exemplifying model of a UAM network along with its graph representation.

By combining the above primitives, different scenarios of UAM networks can be created. An example is shown in Figure 1a. Mathematically, the problem can be formulated as a dynamic network flow model once capacities are known for each sector of the airspace and vertiports at any given time, and solved repeatedly. This fact resembles prior work conducted in [24]. As shown in Figure 1b, a graph $G = (V, E)$ can be defined for a given problem instance. Suppose $S \subset V$ be the set of vertiport source nodes (where flow originates), $T \subset V$ be the set of sink nodes (where flow exits) and $P \subset V$ be the set of all other nodes not in S or T. Then time-varying capacities of each edge can be defined as c^k_{ij} where $(i, j) \in E$ and $k \in 0, \ldots, N$, where N is the total time-step. Let the set of *controllable edges* be defined as $E_c \subset E$ where the value of flow can be directly controlled, and the flow variables be f^k_{ij} for $(i, j) \in E_c$. The aim is to maximize flow over all controllable edges while respecting capacity limits on each edge. This flow problem can now be solved by repeatedly solving an optimization problem at each time-step of a given horizon as capacities change. However, this approach has a number of drawbacks:

- Obtaining the instantaneous capacities for each edge is non-trivial.
- Solving the optimization problem repeatedly may be computationally expensive.

The MFD concept with feedback control aims to remedy these disadvantages, which will be presented in the next section onwards.

III. Methodology

An overview of the methods undertaken for this study is given in Figure 2, which consists of conducting numerous fast-time simulations before and after the proposed departure metering controller is implemented. Data is gathered after each simulation run, mainly in the form of 4D trajectory data. Given such a dataset, a macroscopic model can be derived. Then upon further analysis, controller parameters can be determined and its impact on the microscopic model can be assessed. In order to move forward with the study, both the microscopic and macroscopic model is required. First, the microscopic model is discussed in the next section.

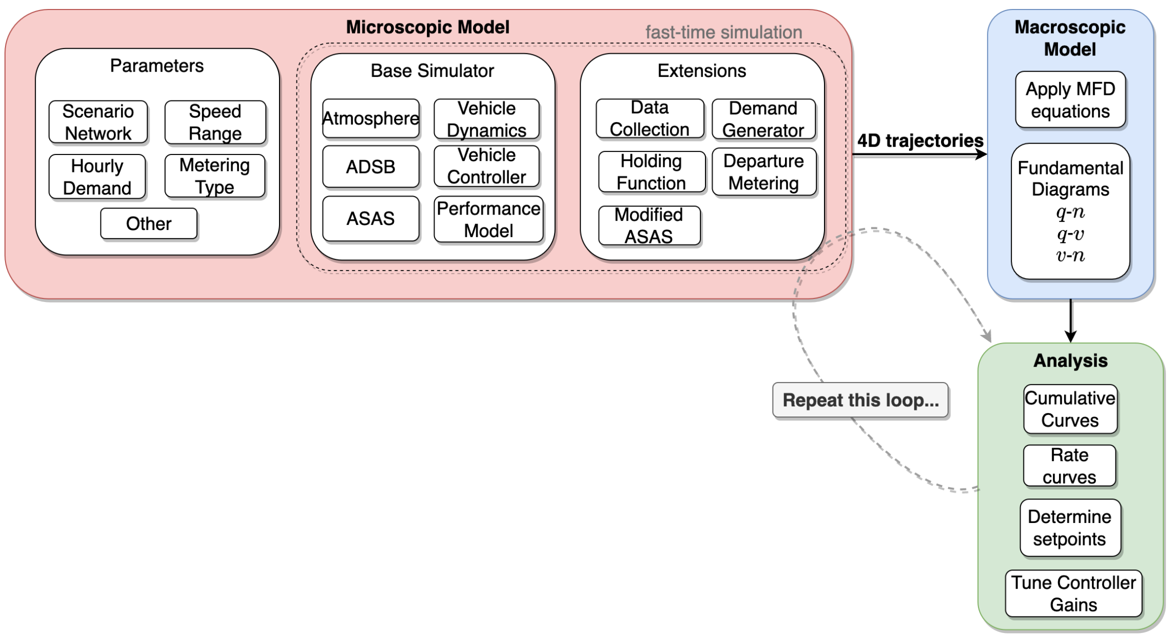

Fig. 2 The simulation under the microscopic model produces 4D trajectories which are used to derive MFD relevant metrics. These quantities are further reduced as parameters for the proposed departure metering controller to schedule vehicle departures at each source vertiport.

A. Microscopic Modeling

A microscopic model aims to simulate individual vehicle units, so that state variables of the models represent an individual's behavior. Such models can often portray traffic flow at a high fidelity, but can be computationally expensive to evaluate or scale.

1. Base Fast-time Simulator

The base version of the BlueSky simulator is used as a starting point to model the behavior of each individual vehicle, from which a macroscopic model can be derived. BlueSky is an open-source air traffic control simulator that provides a platform for research and educational purposes [25]. It was developed with the intention of offering a versatile tool that can be used for studying ATC systems and procedures, as well as for testing and developing new ATM concepts. It offers fast-time simulation capabilities, allowing users to manage air traffic as it unfolds, making it a practical tool for both training and research. The base version of BlueSky provides several components, such as: (i) atmospheric effects on vehicle, (ii) Automatic Dependent Surveillance–Broadcast (ADSB) with noise, (iii) an vehicle separation assurance system, (iv) vehicle dynamics, (v) vehicle controllers for flight management, and (vi) vehicle performance models based on OpenAP and other publicly available data [26–28].

BlueSky allows for the creation of plugins that can be called at periodic intervals. As such, additional features were extended to the simulator for the purposes of this study such as: (i) a customized conflict-resolution algorithm to better allow for speed-up and slow-downs only (no heading change), (ii) a holding function to temporarily remove vehicle from the simulation, and (iii) a departure metering controller whose behavior is configurable by parsing a YAML file.

2. Hourly Demand Generation

An hourly demand generator function was written to simulate vehicle poisson arrivals at each source node. A YAML file defining hourly demand is parsed in and stored as a list, which is used by the generator function. Each time the function is called in BlueSky, a counter queue is incremented according to the number of customer vehicle arrivals. Then, the counter queue is later made available for the departure metering function to modify.

3. Departure Metering Controller

Each i-th source node is also provided with a separate departure metering controller function. Similar to the hourly demand generator function, the controller function is called periodically at a desired rate. The base version of this metering controller (our implementation) will ensure that the necessary separation is met between subsequent departures. The departure separation value is also defined by the user in a YAML file. This metering controller function is implemented as follows:

Algorithm 1: Departure metering controller

```
// This function is called for each i-th source node
while q_i.not_empty() do
    if Using PI metering then
        rate ← Use Eq. (15) to determine desired rate now
        if (t − previous_time_i) > 1/rate then
            break
        end
        previous_time_i ← t
    end
    dist ← compute distance to preceding vehicle AC_{k−1},if any from node_i.
    if dist < threshold_sep then
        Spawn vehicle k in the simulation.
    end
end
```

4. Conflict Detection and Resolution

In this study, state-based conflict detection ([29, 30]) is used to gather all pairwise conflicts, while a custom conflict resolution plugin was written to mainly support speed adjustments. Given a conflict pair, the custom conflict resolution algorithm identifies a leading and following vehicle under any condition. If the leading vehicle is slower than the follower vehicle, it is commanded to speed up. At the same time, the follower vehicle can be commanded to slow down as well. Once the conflict is resolved, the vehicle will resume moving at a self-selected speed.

5. Holding Pattern Function

The last extension to the base version of the BlueSky simulator is a holding pattern function. Since vehicles in this study are not allowed to hover in the corridors, some conflicts may not be resolvable tactically, hence there is a non-zero probability of LOS events. Thus, the purpose of the plugin is to allow any vehicle to temporarily leave the scenario network and go into a "holding" pattern for some time, before returning when safely able. This allows an vehicle to avoid LOS events that would otherwise be imminent if it stayed within the network.

B. Post-Processing for Macroscopic Modeling

The aim of an MFD (also known as NFD or Network Fundamental Diagram) is to showcase relationships between aggregate traffic variables for a given network region. Those variables include average flow and density, mean speed, trip completion rate, and perimeter outflow. The definitions in this paper are adapted from several recent works [6, 10, 31], which were inspired by the seminal work of Edie in 1963 [32]. A large overarching traffic network is typically partitioned into smaller sub-networks, where each one exchanges flow with a neighboring region. Then, an MFD can be extracted for each individual region based on vehicle trajectories. The assumption is that each sub-region experiences congestion in a homogeneous fashion.

The *network average (or aggregated) flow* and *density* can be defined as follows, respectively:

$$Q_{\Delta T} = \frac{1}{S_v \cdot \Delta T} \sum_{\text{veh } i=1}^{N} d_i = \frac{TTD}{S_v \cdot \Delta T} \tag{1}$$

$$K_{\Delta T} = \frac{1}{S_v \cdot \Delta T} \sum_{\text{veh } i=1}^{N} t_i = \frac{TTT}{S_v \cdot \Delta T} \tag{2}$$

In the above equations, ΔT is an analysis time period for which there are N vehicles moving within a network. The variables d_i is the distance (units in [veh · length]) traveled by vehicle i, while variable t_i is the time (units in [veh · time]) spent by vehicle i during the period. Summation of each d_i provides the Total Travel Distance or TTD. Similarly, summation of each t_i provides the Total Travel Time. S_v denotes the volume of the network when considering 3D motion, however for 2D and 1D motion, it can denote area and length respectively. Thus, the units of the aggregated flow and density may be [veh / time], [veh / (length · time)], [veh / (length^2 · time)], or [veh / length], [veh / length^2], [veh / length^3] respectively.

The average flow and density can be transformed into so-called additive variables [31], known as *production* (units in [veh ·length/time]) and *accumulation* or *occupancy* (units in [veh]):

$$P_{\Delta T} = S_v \cdot Q_{\Delta T} = \frac{TTD}{\Delta T} \tag{3}$$

$$n_{\Delta T} = S_v \cdot K_{\Delta T} = \frac{TTT}{\Delta T} \tag{4}$$

These transformed variables allow for aggregation of the properties of many smaller sub-networks (partitions) via a straightforward summation. The production $P_{\Delta T}$ measures the number of trips undertaken by each vehicle per unit time, whereas $n_{\Delta T}$ is the average number of vehicles in the given network during period ΔT.

To obtain the *space-mean speed* or the average speed observed for each vehicle over the length of path, the previous 4 equations can be used as follows:

$$V_{\Delta T} = \frac{Q_{\Delta T}}{K_{\Delta T}} = \frac{P_{\Delta T}}{n_{\Delta T}} = \frac{TTD}{TTT} \tag{5}$$

Equation (5) follows from the fundamental traffic identities via Edie (1963) [32]:

$$Q_{\Delta T} = K_{\Delta T} \cdot V_{\Delta T} \quad \text{or} \tag{6}$$

$$P_{\Delta T} = n_{\Delta T} \cdot V_{\Delta T} \tag{7}$$

The *trip-completion rate* or *throughput* $G_{\Delta T}$ can be measured directly in simulation by tracking all vehicles as they reach their destinations as follows,

$$G_{\Delta T} = \frac{N_{exit}}{\Delta T}, \tag{8}$$

where N_{exit} is the number of vehicles that exit the system.

However, in practice this quantity is difficult to measure outside of simulations due to requiring many sensors. An alternative way to obtain such a quantity is given by the below equation if we assume all vehicles travel the same distance L [33].

$$G(n) = \frac{P(n)}{L} \tag{9}$$

The variable $P(n)$ comes from the fact that according to Daganzo (2007) [33], the MFD can be constructed by treating accumulation n or density k as an independent variable. Thus, we can obtain diagrams for the independent variables $Q(k), V(k)$ or $P(n), V(n)$; in this work, we will use the latter for simplicity.

In [8], an alternate definition of distance is defined: the *effective distance* traveled d_e. This variable measures the achieved distance traveled towards a target, which may be negative if the vehicle is moving away from the target. The definition is motivated by tactical separation maneuvers which may introduce path stretching or rerouting of an vehicle, thereby increasing overall distance traveled. This alone may overestimate the flow Q or production P values. More formally, it is defined as:

$$d_i^e = h_{\Delta t}^{start} - h_{\Delta t}^{end} \tag{10}$$

where $h_{\Delta t}^{start}$ and $h_{\Delta t}^{end}$ is the geodesic distance to the target, at the start and end of the time period Δt respectively, for a given vehicle i. The variable d_i^e can be used in place of d_i in Eqs. (1) and (4). Thus our final equations for post-processing 4D vehicle trajectories is given as follows:

$$P_{\Delta T} = \frac{TETD}{\Delta T} \tag{11}$$

$$n_{\Delta T} = \frac{TTT}{\Delta T} \tag{12}$$

$$V_{\Delta T} = \frac{TETD}{TTT} \tag{13}$$

where $TETD$ is the *total effective travel distance* within a given time period ΔT. Contrary to work performed in [11, 12], a Lagrangian approach is adopted to track the trajectories of each individual vehicle, for the purposes of obtaining the MFD.

C. Analysis for Control Strategy

As mentioned previously in section II, this work assumes outgoing edges for a given vertiport are controllable. Thus, the control objective is to maximize traffic throughput in the overarching network, which is mainly accomplished by maintaining an optimal number of vehicles in the sub-networks by regulating departures. MFD theory shows that this optimum corresponds to the greatest throughput. Once a flow rate has been established for a given edge, vehicle schedules (departure and arrival) can be obtained while also still maintaining separation minima at all times.

One of the simplest control strategy is to limit the departure rate of vehicle based on the current level of vehicle in the network. Using an existing MFD, a discrete-time controller can be used as follows:

$$f_e^k = f_e^{k-1} + K_i(\hat{n} - n_{out}^k) \tag{14}$$

The variable f_e^k represents edge e's flow at the current time step k. The setpoint variable, $\hat{n}$ is obtained from observing an existing MFD, which represents the desired number of vehicle in the network. Next, the variable n_{out}^k is the measured number of vehicle in the network, while K_i is a tuning hyper-parameter that affects controller performance. This control strategy was first demonstrated successfully for ground transportation and is known as ALINEA [34]. As seen above, the controller primarily utilizes integral action via integration of the error $\hat{n} - n_{out}^k$.

Later, an extension of this control strategy incorporated proportional action, which was known as PI-ALINEA [35]. It showcased better responsiveness compared with its predecessor. The discrete-time controller is:

$$f_e^k = f_e^{k-1} + K_i(\hat{n} - n_{out}^k) - K_p(n_{out}^k - n_{out}^{k-1}) \tag{15}$$

The last term represents the additional proportional action, with variable K_p as another tuning hyper-parameter. To protect against integral windup, bounds on the f_e^k should be empirically derived.

Recently, more sophisticated control strategies have been proposed including Model Predictive Control (MPC) and Sliding Mode Control (SMC) [36–38]. However, the present study's focus is on analyzing the impact of a controller on traffic flow management, and not necessarily concerned with finding the best controller. In future work, more advanced controllers can be implemented.

IV. Results and Discussion

A. Setup

The following setup was used for this present study:

- All vehicles enter the network at a speed that is uniformly sampled from an interval. For a given source vertiport, a path to the destination is randomly sampled from the k-shortest paths, where $k = 3$, and provided to the vehicle for waypoint following.
- The ADSB system includes a built-in noise model; this was not modified during simulations.
- Vehicles can enter a holding pattern at any time and also return to the network if safely able. A vehicle's holding time is reset if it is considered for re-entry, but cannot do so due to a potential LOS.
- Only 1 type of vehicle is considered in this study: the Amazon Drone from Bluesky's library.
- A simulation timestep of 0.05 seconds was used for all experiments.
- A value of 200 meters was used for basic departure separation.
- Data collection was gathered at 1Hz.
- Wind is not considered in this study.
- The controller gains used are $K_p = 1$ and $K_i = 1$ respectively.
- There are no arrival rate limits imposed on vertiports.

A scenario consists of a directed, connected graph, indicating which nodes are sources and sinks. Additionally, an hourly demand list is given for each source node. Given this, several trial simulations were performed using the above assumptions.

B. Scenario Overview

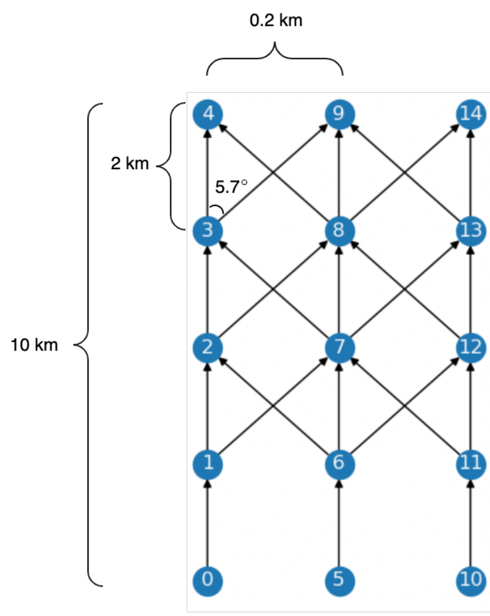

Fig. 3 A multi-lane scenario with source and destination vertiport nodes. Note the network is not drawn to scale.

The scenario considered in this study was selected based on real-world applicability, as shown in Figure 3. The scenario includes a multi-lane sky corridor, where vehicles simulate a lane-change by following specifically placed waypoints. The flow originates at the source vertiport nodes and exits at destination vertiport nodes. In this scenario as shown in Figure 3, a lattice graph is defined over a 4km^2 area, with a lane spacing of 200m and a longitudinal spacing of 2km between nearby nodes. Additionally, directed edges connect nodes to those that are positioned ahead longitudinally across various lanes. Source vertiport nodes are labeled 0, 5, and 10, while destination vertiport nodes are labeled 4, 9, and 14. The dimensions of the segments were chosen to avoid vehicles making sharp turns during waypoint following. As mentioned, vehicles simulate lane-changing behavior by following a given set of waypoints that may be spread out consecutively between different lanes.

Table 1 ***multi-lane*** **scenario: Vehicle demand rates [veh/hour] for each hour of the simulation.**

	Hr 0	Hr 1	Hr 2	Hr 3	Hr 4	Hr 5	Hr 6	Hr 7	Hr 8	Hr 9
Vertiport 0	50	150	150	150	400	400	400	400	400	50
Vertiport 5	50	50	150	150	150	400	400	400	50	50
Vertiport 10	50	50	50	150	150	150	400	50	50	50

The demand rate originating at each source vertiport is given in Table 1 and involves ramping up to a maximum of 400 vehicles per hour before decreasing to 50. The range of values were chosen empirically based on initial loading experiments.

C. Macroscopic Fundamental Diagrams

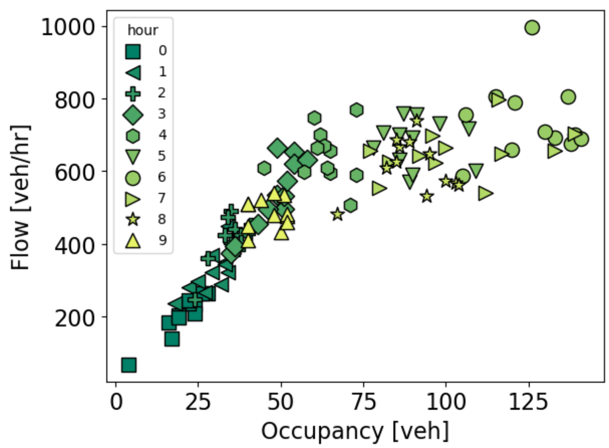

(a)

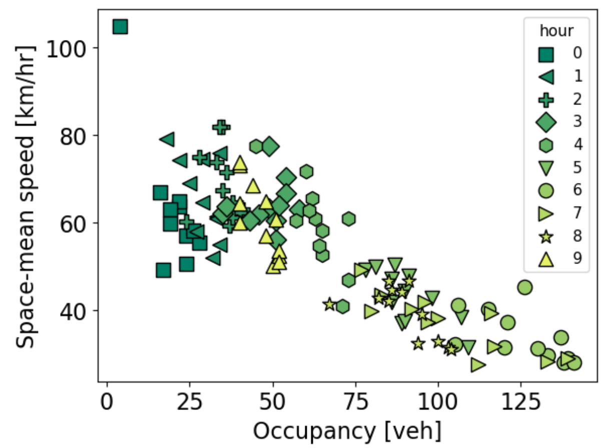

(b)

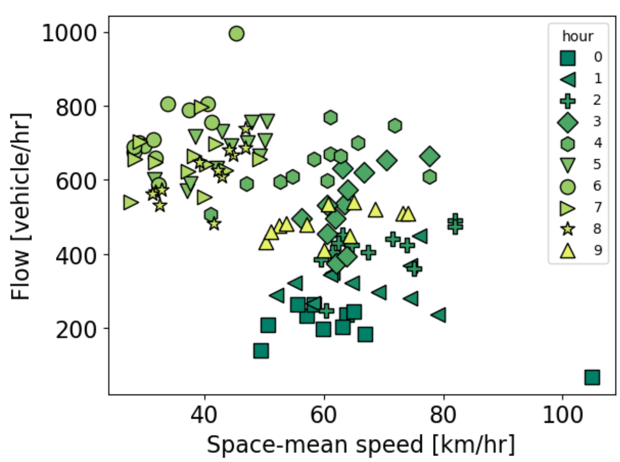

(c)

Fig. 4 Macroscopic fundamental diagrams for the "multi-lane" scenario consisting of flow vs. occupancy (a), ground speed vs. occupancy (b), and flow vs. ground speed (c).

All MFD are generated with a sliding time window of 5 minutes over the vehicle trajectory data (ΔT) using Eqs. (11)-(13), along with Eq. (8). A penalty factor on the distance traveled for a vehicle in holding was introduced to mimic a vehicle moving away from the destination, thereby penalizing flow values. Additionally in this work, only a single MFD was generated per scenario network, i.e. graph partitioning was not necessary. Afterward, the MFD of each scenario was used to determine a occupancy setpoint for the proposed controller. The MFD for scenario *multi-lane* is given in Figure 4. In the flow vs. occupancy plot, flow increases freely and linearly from 0 to 600 vehicles per hour, corresponding to 0 to 60 vehicles in occupancy. Additionally, the data exhibits low scatter in this linear region indicating homogeneous traffic conditions throughout the network. Beyond the linear region, the plot exhibits more scatter and appears to saturate around a mean of 600 vehicles per hour. The data also does not appear to trend downward, suggesting that any further increase in occupancy may not lead to congestion in the traditional sense, i.e. zero-velocity traffic. Based on the shape of this plot, a setpoint of 60 vehicles was chosen, since any further occupancy increase resulting in diminishing returns on flow.

In the next subplot of the MFD, concerning ground speed vs. occupancy in Figure 4a, the data trends downward with increasing occupancy. This makes sense since high occupancy can lead to a higher probability of conflicts, requiring more vehicles to adjust their speeds or even go into holding.

For the final MFD subplot as shown in Figure 4c, the relationship between flow and ground speed trends downward, but is more subtle due to the data clustering around 3 regions. This clustering effects suggests that the vehicles were not able to traverse the network at a wide range of speeds. Nonetheless, the downward trend suggests that a majority of traffic flow occurs at lower speeds rather than higher.

D. Impact of Controller Metering on Source Departures

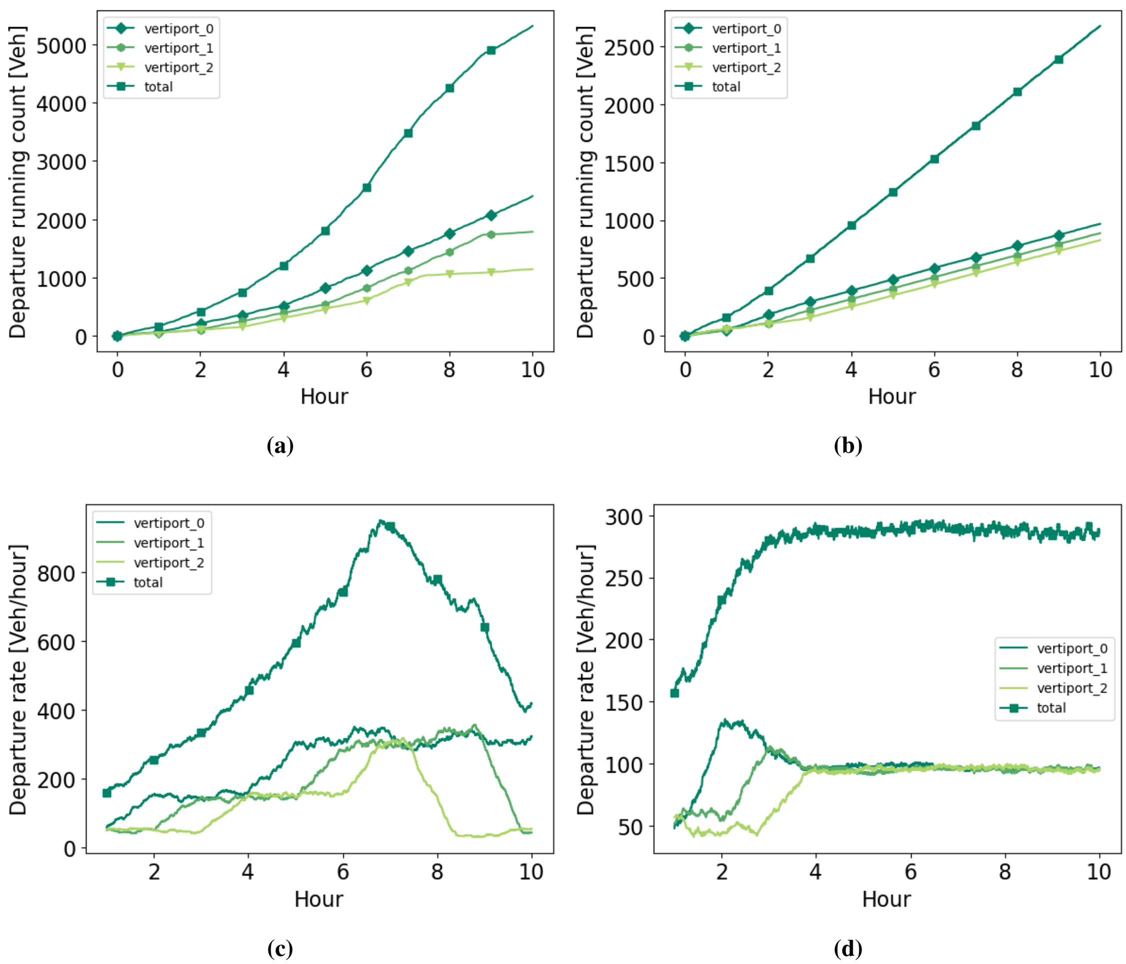

Fig. 5 Cumulative (top) and rate of departures (bottom) for the *multi-lane* scenario comparing open-loop (left) and closed-loop responses (right).

Figure 5 shows the effect of using the controller to meter departures at each of the source nodes for the *multi-lane* scenario. Cumulative curves for the departures are shown in the top subfigures, which track the running number of departures over time. Without using the controller (left), the total number of departures reaches over 5000 vehicles at the 10th hour of the simulation, compared to just over 2500 when the controller is used (right). The bottom subfigures show the individual and total departure rate, obtained by taking the time derivative of the cumulative curves. Without the controller, the total departure rate increases to a peak beyond 800 vehicles/hour (left). However, with the controller, the departure rate displays an asymptotic response and levels out to about 275 vehicles/hour throughout the simulation.

E. Impact of Controller Metering on Source Departure Queue Length

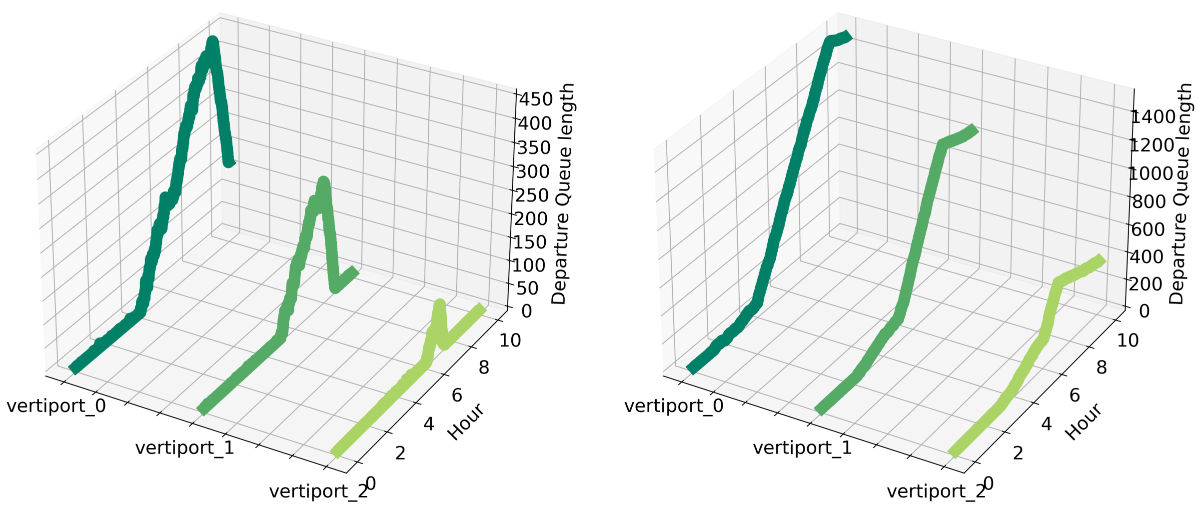

(a) **(b)**

Fig. 6 Departure queue length for the *multi-lane* scenario, comparing open-loop (left) and closed-loop responses (right).

The departure queue length at any given time is shown in Figure 6 for the present scenario, with and without the use of a controller. In Figure 6a, the departure queue length is shown without controller use. The queue length over time for vertiports 0, 1, and 2 peak at approximately 450, 300, and 100 vehicles, respectively. These trends roughly follow the same hourly demand from Table 1. Comparatively, employing a controller results in higher departure queue length as shown in Figure 6b. The queue length for vertiports 0, 1, and 2 now peak at approximately 1400, 1000, and 400 vehicles respectively. The queue length increases under a controller because the departure rate has decreased.

F. Impact of Controller Metering on Destination Arrivals

Figure 7 illustrates the cumulative and rate of arrivals to the destination vertiports in the *multi-lane* scenario. In the baseline (left) subfigure without the controller, the total cumulative arrivals reach to just over 1750 vehicles. Comparatively, the cumulative arrivals for the controller-based scenario (right) only reaches to just over 1400 vehicles. The baseline has a higher cumulative arrival curve due to having a higher rate of arrivals as seen in the bottom subfigures, with a peak rate of nearly 300 vehicles/hour and minimum of about 150 vehicles/hour. Compared to the baseline, the arrival rate of the controller-based benchmark levels off about 150 vehicles/hour. Clearly the use of the proposed control strategy limits the throughput by about 20%.

G. Impact of Controller Metering on Vehicle Occupancy

Various vehicle count metrics at any given time are shown in Figure 8, for the *multi-lane* scenario presented in this study. Those metrics are: (i) the total number of vehicles in the entire simulation at a given time (total), (ii) the number of vehicles in the simulation graph network at a given time (in-network), and (iii) the number of vehicles in holding at

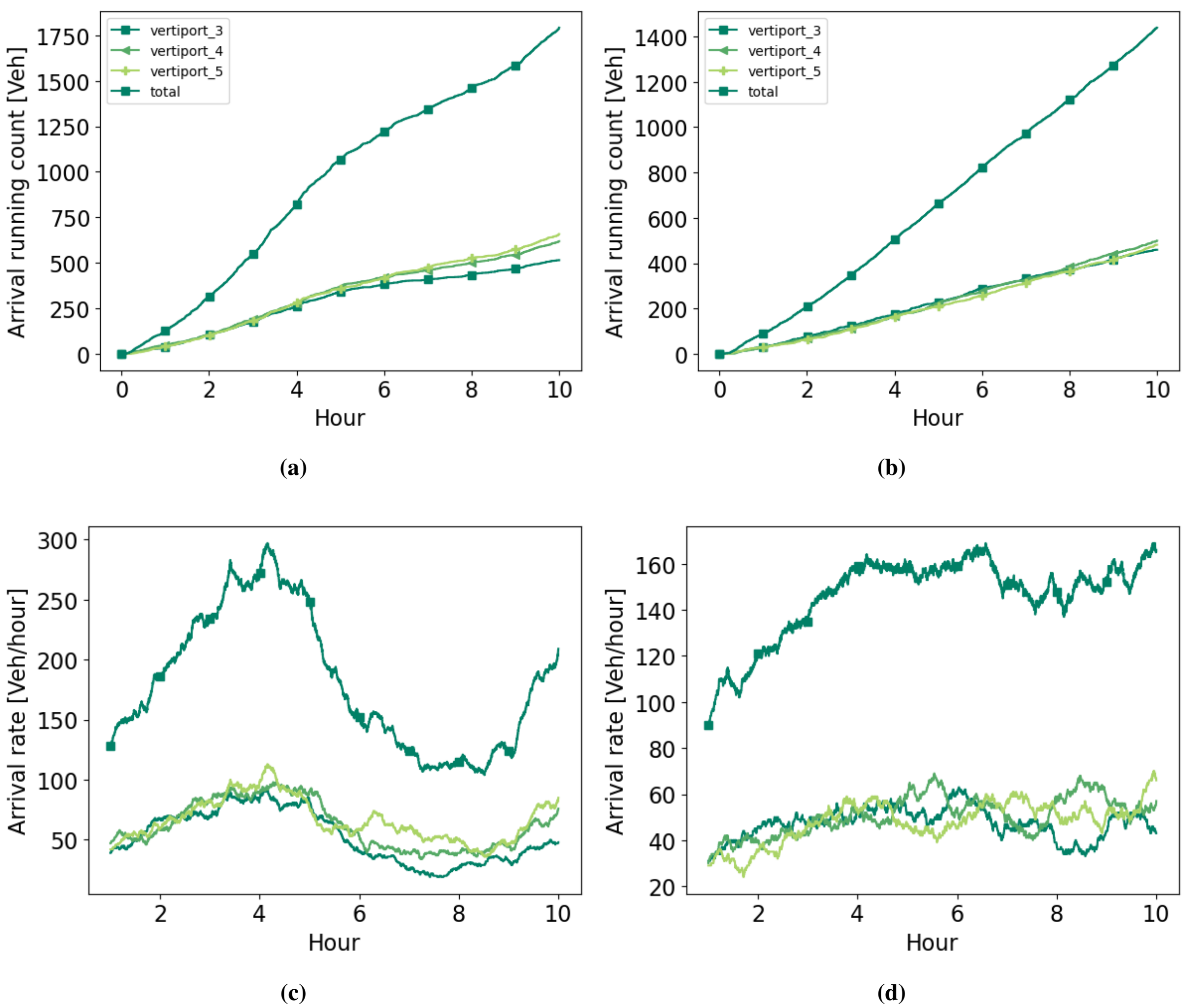

Fig. 7 Destination arrival running count and rate for the *multi-lane* scenario, comparing open-loop (top) and closed-loop responses (bottom).

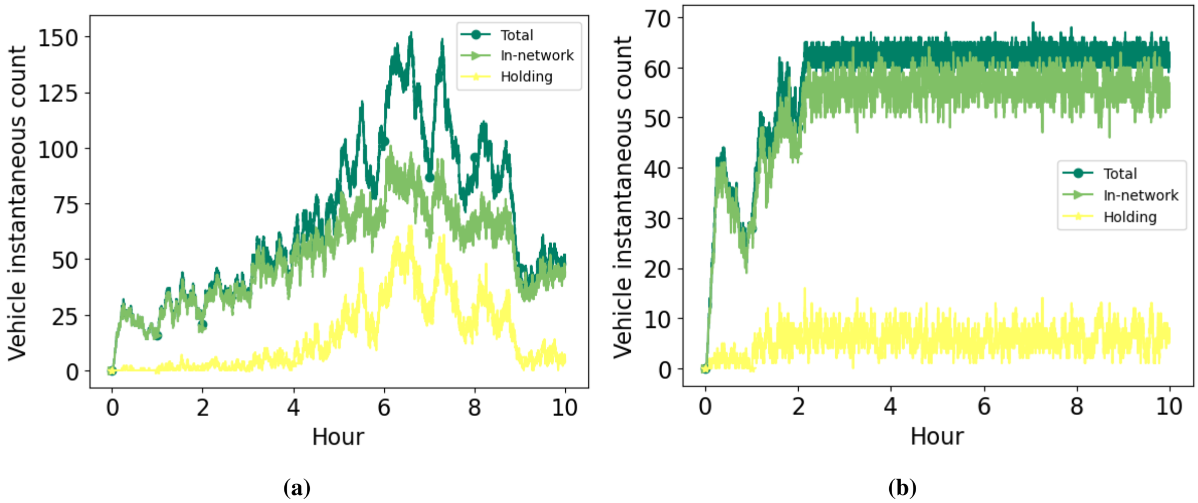

Fig. 8 Vehicle running count for the "multi-lane" scenario, comparing open-loop (left) and closed-loop responses (right).

a given time (holding). Note that the total count is equal to the sum of in-network and holding counts. Without the proposed metering controller, the total vehicle count fluctuates with the hourly demand and reaches about 140 briefly around the 6 hour mark as shown in Figure 8a. Additionally, there are at most about 60 vehicles in holding. Contrasting this, the scenario under the proposed metering controller exhibits a constant number of vehicles in the simulation, as shown in Figure 8b. Additionally, the number of vehicles in holding is on average 8. Clearly, the metering controller is able to reduce the peak number of vehicles in holding by about 80% in the studied scenario, albeit at a slight cost to throughput (20%).

V. Conclusions

In this study, a structured airspace network was developed, consisting of a multi-lane, lane-changing scenario. Macroscopic Fundamental Diagram (MFD) theory was used to successfully capture macroscopic traffic variables such as flow, speed, and occupancy. Under this framework, the scenario was loaded with traffic at an increasing demand rate. After the MFD was generated, a setpoint for the scenario was determined and given to several decentralized departure rate controllers, located at each vertiport for the purposes of metering. The controllers were able to regulate overall traffic levels or occupancy to the desired setpoint. Though the overall traffic throughput was impacted to a degree, the number of vehicle in holding dropped significantly. Additionally, the arrival rate is more consistent, not suffering from large fluctuations.

Future work will be focused on investigating more realistic, complex, and larger scenarios. For instance, arrival rates may be imposed on vertiports, along with dynamic network configurations due to weather. Additionally, more efficient implementations of the conflict detection and conflict resolution algorithm is necessary for faster data gathering. The holding zone can also be implemented in the simulation instead of assuming a fixed and reset-able holding time.

VI. Acknowledgment

The authors would like to thank subject matter experts at the FAA office of NextGen for their valuable comments and feedback.

References

[1] Federal Aviation Administration, "Urban Air Mobility (UAM) Concept of Operations, Version 2.0," , 2023. URL `https://www.faa.gov/sites/faa.gov/files/Urban%20Air%20Mobility%20%28UAM%29%20Concept%20of%20Operations%202.0_0.pdf`, accessed: 2023-11-8.

[2] Bauranov, A., and Rakas, J., "Designing airspace for urban air mobility: A review of concepts and approaches," *Progress in Aerospace Sciences*, Vol. 125, 2021, p. 100726.

[3] Jung, J., Rios, J. L., Xue, M., Homola, J., and Lee, P. U., "Overview of NASA's Extensible Traffic Management (xTM) Research," *AIAA SciTech Forum*, , No. 1916, 2022.

[4] Godfrey, J., "The mechanism of a road network," *Traffic Engineering & Control*, Vol. 8, No. 8, 1969.

[5] Geroliminis, N., and Daganzo, C. F., "Existence of urban-scale macroscopic fundamental diagrams: Some experimental findings," *Transportation Research Part B: Methodological*, Vol. 42, No. 9, 2008, pp. 759–770.

[6] Tereshchenko, I., *Demand Prediction and Capacity Modelling for Applications in En Route Air Traffic Management*, University of California, Berkeley, 2021.

[7] Jang, D.-S., Ippolito, C. A., Sankararaman, S., and Stepanyan, V., "Concepts of airspace structures and system analysis for uas traffic flows for urban areas," *AIAA Information Systems-AIAA Infotech@ Aerospace*, 2017, p. 0449.

[8] Tereschenko, I., Hanson, M., and Zou, B., "Macroscopic Fundamental Diagram for Air Traffic: Preliminary Theoretic Results and Simulation Findings," *Proc., International Conference for Research in Air Transportation,(virtual)*, 2020.

[9] Cummings, C., and Mahmassani, H., "Emergence of 4-D system fundamental diagram in urban air mobility traffic flow," *Transportation Research Record*, Vol. 2675, No. 11, 2021, pp. 841–850.

[10] Safadi, Y., Fu, R., Quan, Q., and Haddad, J., "Macroscopic fundamental diagrams for low-altitude air city transport," *Transportation Research Part C: Emerging Technologies*, Vol. 152, 2023, p. 104141.

[11] Menon, P., Sweriduk, G., Lam, T., Cheng, V., and Bilimoria, K., "Air traffic flow modeling, analysis and control," *AIAA Guidance, Navigation, and Control Conference and Exhibit*, 2003, p. 5712.

[12] Menon, P. K., Sweriduk, G. D., and Bilimoria, K. D., "New approach for modeling, analysis, and control of air traffic flow," *Journal of guidance, control, and dynamics*, Vol. 27, No. 5, 2004, pp. 737–744.

[13] Lighthill, M., and Whitham, G., "On Kinematic Waves. I, Volume Movement in Long Rivers. II, A Theory of Traffic Volume on Long Crowded Roads," *Proceedings of the Royal Society of London*, Vol. 229, No. 1178, 1955.

[14] Roy, S., Sridhar, B., and Verghese, G. C., "An aggregate dynamic stochastic model for an air traffic system," *Proceedings of the 5th Eurocontrol/Federal Aviation Agency Air Traffic Management Research and Development Seminar, Budapest, Hungary*, 2003.

[15] Sridhar, B., Soni, T., Sheth, K., and Chatterji, G., "Aggregate flow model for air-traffic management," *Journal of Guidance, Control, and Dynamics*, Vol. 29, No. 4, 2006, pp. 992–997.

[16] Wang, Z., Delahaye, D., Farges, J.-L., and Alam, S., "A quasi-dynamic air traffic assignment model for mitigating air traffic complexity and congestion for high-density UAM operations," *Transportation Research Part C: Emerging Technologies*, Vol. 154, 2023, p. 104279.

[17] Wang, Z., Delahaye, D., Farges, J.-L., and Alam, S., "Complexity optimal air traffic assignment in multi-layer transport network for Urban Air Mobility operations," *Transportation Research Part C: Emerging Technologies*, Vol. 142, 2022, p. 103776.

[18] Vascik, P. D., and Hansman, R. J., "Development of vertiport capacity envelopes and analysis of their sensitivity to topological and operational factors," *AIAA Scitech 2019 Forum*, 2019, p. 0526.

[19] Roy, S., Kotwicz Herniczek, M. T., Leonard, C., Jha, A., Wang, N., German, B., and Garrow, L., "A multi-commodity network flow approach for optimal flight schedules for an airport shuttle air taxi service," *AIAA Scitech 2020 Forum*, 2020, p. 0975.

[20] Wei, Q., Nilsson, G., and Coogan, S., "Scheduling of urban air mobility services with limited landing capacity and uncertain travel times," *2021 American Control Conference (ACC)*, IEEE, 2021, pp. 1681–1686.

[21] Shihab, S. A. M., Wei, P., Ramirez, D. S. J., Mesa-Arango, R., and Bloebaum, C., "By schedule or on demand?-a hybrid operation concept for urban air mobility," *AIAA Aviation 2019 Forum*, 2019, p. 3522.

[22] Lee, H., Moolchandani, K. A., and Arneson, H., "Demand capacity balancing at vertiports for initial strategic conflict management of urban air mobility operations," *2022 IEEE/AIAA 41st Digital Avionics Systems Conference (DASC)*, IEEE, 2022, pp. 1–10.

[23] Chen, S., Evans, A., Brittain, M., and Wei, P., "Integrated Conflict Management for UAM with Strategic Demand Capacity Balancing and Learning-based Tactical Deconfliction," *arXiv preprint arXiv:2305.10556*, 2023.

[24] Zawack, D. J., and Thompson, G. L., "A dynamic space-time network flow model for city traffic congestion," *Transportation Science*, Vol. 21, No. 3, 1987, pp. 153–162.

[25] Hoekstra, J. M., and Ellerbroek, J., "Bluesky ATC simulator project: an open data and open source approach," *Proceedings of the 7th international conference on research in air transportation*, Vol. 131, FAA/Eurocontrol USA/Europe, 2016, p. 132.

[26] Sun, J., Hoekstra, J. M., and Ellerbroek, J., "Estimating aircraft drag polar using open flight surveillance data and a stochastic total energy model," *Transportation Research Part C: Emerging Technologies*, Vol. 114, 2020, pp. 391–404.

[27] Sun, J., Ellerbroek, J., and Hoekstra, J. M., "WRAP: An open-source kinematic aircraft performance model," *Transportation Research Part C: Emerging Technologies*, Vol. 98, 2019, pp. 118 – 138. https://doi.org/https://doi.org/10.1016/j.trc.2018.11.009.

[28] Developer, X., "Data Development Documentation," , 2023. URL https://developer.x-plane.com/docs/data-development-documentation/.

[29] Hoekstra, J. M., and Ellerbroek, J., "Aerial robotics: State-based conflict detection and resolution (detect and avoid) in high traffic densities and complexities," *Current Robotics Reports*, Vol. 2, No. 3, 2021, pp. 297–307.

[30] Bach, R., Farrell, C., and Erzberger, H., "An algorithm for level-aircraft conflict resolution," *NASA, Tech. Rep. CR-2009-214573*, 2009.

[31] Mariotte, G., "Dynamic modeling of large-scale urban transportation systems," Ph.D. thesis, Université de Lyon, 2018.

[32] Edie, L. C., et al., *Discussion of traffic stream measurements and definitions*, Port of New York Authority New York, 1963.

[33] Daganzo, C. F., "Urban gridlock: Macroscopic modeling and mitigation approaches," *Transportation Research Part B: Methodological*, Vol. 41, No. 1, 2007, pp. 49–62.

[34] Papageorgiou, M., Hadj-Salem, H., Blosseville, J.-M., et al., "ALINEA: A local feedback control law for on-ramp metering," *Transportation research record*, Vol. 1320, No. 1, 1991, pp. 58–67.

[35] Kan, Y., Wang, Y., Papageorgiou, M., and Papamichail, I., "Local ramp metering with distant downstream bottlenecks: A comparative study," *Transportation Research Part C: Emerging Technologies*, Vol. 62, 2016, pp. 149–170.

[36] Safadi, Y., Geroliminis, N., and Haddad, J., "Aircraft Departures Management for Low Altitude Air City Transport based on Macroscopic Fundamental Diagram," *2023 American Control Conference (ACC)*, 2023, pp. 4393–4398.

[37] Haddad, J., Mirkin, B., and Assor, K., "Traffic flow modeling and feedback control for future Low-Altitude Air city Transport: An MFD-based approach," *Transportation Research Part C: Emerging Technologies*, Vol. 133, 2021, p. 103380.

[38] Bichiou, Y., Elouni, M., Abdelghaffar, H. M., and Rakha, H. A., "Sliding mode network perimeter control," *IEEE Transactions on Intelligent Transportation Systems*, Vol. 22, No. 5, 2020, pp. 2933–2942.